THE EUROPEAN
PHYSICAL JOURNAL D

Regular Article - Atomic and Molecular Collisions

High kinetic energy-ion mobility spectrometry-mass spectrometry investigations of several volatiles and their fully deuterated analogues

Florentin Weiss[1,a] , Gary Eiceman[2,3], Tilmann D. Märk[4], Chris A. Mayhew[1,5] , Veronika Ruzsanyi[1] ,
Christoph Schaefer[6] , and Stefan Zimmermann[6]

[1] Institute for Breath Research, University of Innsbruck, Innrain 66, 6020 Innsbruck, Austria
[2] Department of Chemistry and Biochemistry, New Mexico State University, Las Cruces, NM 88003, USA
[3] Department of Chemistry, VERIFIN, Finnish Institute for the Verification of the Chemical Weapons Convention, University of Helsinki, 00014 Helsinki, Finland
[4] Institute for Ion Physics and Applied Physics, University of Innsbruck, 6020 Innsbruck, Austria
[5] Tyrolean Cancer Research Institute, Innrain 66, 6020 Innsbruck, Austria
[6] Institute of Electrical Engineering and Measurement Technology, Leibniz University Hannover, 30167 Hannover, Germany

© The Author(s) 2022, corrected publication 2023

Abstract. The first High Kinetic Energy-Ion Mobility Spectrometry-Mass Spectrometry (HiKE-IMS-MS) studies involving six volatiles (acetone, acetonitrile, methanol, ethanol, 2-propanol, and 1-butanol) and their fully deuterated analogues are reported. The goal is to further our understanding of the ion–molecule chemistry occurring in the HiKE-IMS. This is needed for its full analytical potential to be reached. Product ions are identified as a function of the reduced electric field (30–115 Td) and the influence of sample air humidity in the reaction region on deuterium/hydrogen (D/H) exchange reactions is discussed. Reagent ions include $H_3O^+(H_2O)_m$ ($n = 0, 1, 2$ or 3), $NO^+(H_2O)_n$ ($m = 0$ or 1) and $O_2^{+\cdot}$. Reactions with $H_3O^+(H_2O)_m$ lead to protonated monomers (through either proton transfer or ligand switching). Reactions with NO^+ involve association with acetone and acetonitrile, hydride anion abstraction from ethanol, 2-propanol, and 1-butanol, and hydroxide abstraction from 2-propanol and 1-butanol. With the exception of acetonitrile, $O_2^{+\cdot}$ predominantly reacts with the volatiles via dissociative charge transfer. A number of sequential secondary ion-volatile processes occur leading to the formation of dimer and trimer-containing ion species, whose intensities depend on a volatile's concentration and the reduced electric field in the reaction region. Deuterium/hydrogen (D/H) exchange does not occur for product ions from acetone-d_6 and acetonitrile-d_3, owing to their inert methyl functional groups. For the deuterated alcohols, rapid D/H-exchange reaction at the hydroxy group is observed, the amount of which increased with the increasing humidity of the sample air and/or lowering of the reduced electric field.

1 Introduction

The human volatilome consists of hundreds of different volatile organic compounds (VOCs), whose origins are mainly endogenous, but also having contributions from exogenous sources [1]. Sweat, urine, saliva, skin and breath are suitable paths for the release of these VOCs from the body. Among others, breath volatile analysis represents a promising method for use in the early detection and screening of diseases or for monitoring metabolic changes in the human body [2]. Unlike other diagnostic techniques, for example blood analysis or biopsies, breath sampling is distinguished by being non-invasive and pain-free [3]. A major challenge to develop breath volatile tests is that the composition of exhaled breath depends on various factors such as environmental, age, physical activity, diet, body mass index, sex, co-morbidities and smoking behavior [4]. This complicates the use of chemical fingerprinting for the identification of biochemical or metabolic pathways and markers. In addition, an insufficient understanding of the origin of the endogenous volatile markers for diseases further limits application.

We wish to dedicate this paper to Professor Kurt Becker on the occasion of his upcoming 70th birthday. Kurt's interests lie in both pure and applied research, both of which are featured in this paper.

[a] e-mail: florentin.weiss@uibk.ac.at (corresponding author)

Difficulties of breath analysis using endogenous volatiles can be overcome by the use of isotopically labeled substances, which are either ingested, absorbed or inhaled. If volatile, trace levels of these substrates, and any associated trace volatile metabolites, can be measured on exhaled breath, applications of which include pharmacokinetic studies for use in medical diagnosis. A prominent example of metabolic volatile profiling with isotopically labelled substrates is the LiMAx test, which provides a measure of liver function [5]. Based on the hepatocyte-specific metabolism, ingested ^{13}C-labeled methacetin is rapidly metabolized by the cytochrome P450 1A2 enzyme to acetaminophen and $^{13}CO_2$, with the latter being exhaled pulmonary. This leads to an increased $^{13}CO_2$:$^{12}CO_2$ ratio in exhaled breath, and significantly more so for healthy people compared to people suffering from impaired liver function. Another well-known use of isotope labelling is the ^{13}C-urea breath test for the detection of *Helicobacter pylori*. The presence of *Helicobacter pylori* infection can also be determined from the increase in the $^{13}CO_2$:$^{12}CO_2$ ratio in exhaled breath [6].

For these tests to be successful, sufficient $^{13}CO_2$ needs to be generated that can be recorded above the normal high level always present in exhaled breath. To achieve this, substantial quantities of an isotopically labelled compound need to be ingested (e.g. 75 mg of ^{13}C-urea is required for the *Helicobacter pylori* test [6]). Such high quantities substantially adds to the cost of the tests, and, depending on the isotopically labelled substrate, can potentially lead to side effects.

Deuterium labelled substrates present an interesting alternative to increase the potential scope of application to track metabolism, because the compound and its metabolites produced would be unique, and thus lower amounts of a substrate would be required. The potential of deuterium labelling has been highlighted in a Proton Transfer Reaction-Time-of-Flight-Mass Spectrometer (PTR-ToF–MS) study by Ruzsanyi et al. [7]. They demonstrated the use of a deuterium labeled 2-propanol in a breath test to determine its oxidation by liver alcohol dehydrogenase to acetone-d_3. Importantly, only 0.8 mg of 2-propanol-d_3 had to be swallowed in order to detect protonated acetone-d_3 in the exhaled breath for several hours following ingestion.

The successful use of deuterium labeled volatile substrate breath tests requires an understanding as to how these and their volatile metabolites chemically behave within a given analytical device, especially in the presence of high water concentration, which will occur when analyzing humid exhaled breath samples. The presence of water can lead to significant D/H exchange with the deuterium containing product ions, which would complicate the chemical analysis and reduce analytical sensitivity.

Recently, Mochalski et al. reported a systematic PTR-ToF–MS investigation of nine deuterated volatile compounds [8]. The product ion formation was studied at two relative humidity levels of ~ 0.5 and 100% within the drift (reaction) region, with a key aim to investigate the influence of humidity in the drift tube on the primary deuterium containing product ions. Measurements were performed at reduced electric field, E/N, values of between 80 and 150 Td; where E is the electric field strength in units of V m^{-1} and N is the gas number density in the drift (reaction) tube in units of m^{-3}, and 1 Td Townsend = 10^{-21} V m^2. Mochalski et al. showed that D/H exchange depends not only on the humidity in the drift tube and E/N, as expected, but also on the structure of the reactant neutral. For example, following proton transfer, D/H exchange reactions between the protonated parent and H_2O are not facile for compounds that have deuterated methyl groups. Thus, increases in sample gas humidity had no effect on protonated acetone-d_6 ($C_3D_6OH^+$, m/z 65.087). In comparison, following proton transfer to fully deuterated 2-propanol, significant D/H exchange was observed to occur, which increased with increasing humidity in the reaction region. A similar behavior was also observed for fully deuterated ethanol.

Here we extend the earlier PTR-ToF–MS study of Mochalski et al. to investigate ion–molecule reactions of several volatiles and their deuterated analogues using a High Kinetic Energy-Ion Mobility Spectrometry-Mass Spectrometry (HiKE-IMS-MS). The volatiles included in this study are acetone (C_3H_6O), acetone-d_6, acetonitrile (C_2H_3N), acetonitrile-d_3, methanol (CH_3OH), methanol-d_4, ethanol (C_2H_5OH), ethanol-d_6, 2-propanol (C_3H_7OH), 2-propanol-d_8, 1-butanol (C_4H_9OH), and 1-butanol-d_{10}.

There are only a few studies that have investigated ion–molecule chemistry and product ion formation occurring in the reaction region of the HiKE-IMS. Hence, an orderly and systematic examination of numerous analytes is essential to increase our knowledge of the gas phase ion processes. A major goal of this work is to provide further underpinning fundamental studies to improve our understanding of the ion–molecule chemistry occurring, and hence ascertain in more detail the HiKE-IMS's potential as a new analytical tool. With this goal in mind, the volatiles mentioned above have been investigated using both relatively *dry* and *humid* sample air, with the latter being comparable to that found in exhaled breath, and employing a range of E/N values. We provide detailed information on the product ions (primary and secondary) formed within the reaction region of the HiKE-IMS, and the studies of the deuterated substances deliver information on D/H-exchange.

2 Methods

2.1 High kinetic energy-ion mobility spectrometry-mass spectrometry (HiKE-IMS-MS)

Information on the HiKE-IMS, the time-of-flight mass spectrometer, and the operational parameters used have already been published in detail elsewhere [9–11]. Here we provide an overview pertinent to this study.

Compared to atmospheric pressure IMS systems, the HiKE-IMS operates at much lower pressures (in this study we used 14 mbar). This means that at the maximum drift voltage available, an E/N strength of 115 Td can be achieved, which is comparable to the normal operating value used in the majority of PTR-ToF–MS measurements. The value of E/N is an important operational parameter, because it controls the mean drift speed of the ions in the drift tube, and hence determines the collisional energies between ions (reagents and products) and neutral species and controls the reaction times.

The HiKE-IMS was operated at room temperature, which was typically around 30 °C. The sample air flow, whose inlet is located in the reaction region opposite to the ionisation source, which is a corona discharge operated at 1050 V, was maintained at 15 mL_s/min (millilitre standard per minute). The drift region airflow was introduced near the end of the drift tube using an inlet flow of 24 mL_s/min. Both air streams flow in the same direction, being pumped out of the instrument at the front of the ionisation source/reaction region using a membrane pump (MVP-40, Pfeiffer Vacuum), which was connected to the front end (the corona discharge region) of the HiKE-IMS. A gas-dosing valve, an EVN-116 from Pfeiffer Vacuum, controls the total outlet gas flow. The pressure inside the HiKE-IMS was monitored using a capacitive gauge (CMR-362, Pfeiffer Vacuum). The lengths of the ionisation source/reaction and drift regions are 105 and 153.5 mm, respectively. With the voltage supplies provided for the reaction and drift regions being able to supply 1–4 and 2–6 kV, respectively, an E/N range of 30–115 Td could be applied throughout the whole of the drift tube (i.e., to both ionisation source/reaction and drift regions).

Information on the ion–molecule chemistry occurring in the HiKE-IMS is obtained by identifying the reagent and product ions and their intensities measured with a home-built ToF–MS. This ToF–MS contains an orthogonal acceleration path, based on the Wiley-McLaren arrangement, with a short linear field free flight path of only 28.5 cm. A micro channel plate is used to detect the ions. The lack of a reflectron and the short field free region results in low temporal and hence low mass resolution. The ToF–MS mass resolution ($m/\Delta m$) is only about 80 at m/z 100. However, this is usually sufficient to provide reasonably accurate peak positions, and given that for this study the compounds being introduced into the reaction region are known, the molecular formulae of the reagent and product ions can usually be determined with a high level of confidence. An advantage of working with this TOF–MS is that the transfer optics from the HiKE-IMS to the MS do not provide additional translational energy to the ions thereby limiting dissociation of the cluster ions upon transfer into the detection region. However, low mass resolution issues did cause problems for determining the intensities of deuterated product ions that had undergone sequential D/H exchange. The impact of this is discussed later in the results' section. We just comment here that because of the low mass resolution, product

ions separated by 1 amu, i.e., those associated with D/H exchange, could not be completely resolved. This meant that only semi-quantitative comparisons between products ions resulting from the unlabeled and deuterated alcohols could be made. This is reflected in the product ion distributions presented as a function of E/N. The ToF–MS spectrum-to-spectrum acquisition rate was set to 50 Hz.

After migrating down the drift tube under the influence of the applied electric field, a percentage of the reagent and product ions exit the drift tube of the HiKE-IMS via metal plate containing a pinhole of 0.8 mm diameter at its centre, which is located after a three-grid construction. From there, they enter a linear transfer ion-optics region, which is maintained at a pressure of 3×10^{-3} mbar by the use of a turbo molecular pump (Pfeiffer Vacuum, HiPace 300). The ions are then drawn towards a skimmer cone, which is placed at a distance of 20 mm from the three-grid construction. They pass through this skimmer via a central hole of diameter 1.0 mm, thereby transferring the ions into the ToF–MS. Using the turbo molecular pump that also upholds the vacuum in the transfer region, the ToF–MS is maintained at a pressure of about 6×10^{-6} mbar. The pressures of the two high-vacuum regions are determined using a compact full range Pirani and cold cathode gauge (Pfeifer Vacuum, PKR 251). The ToF–MS is calibrated with known ions so that the arrival flight times of the unknown ions at the detector can be converted to individual m/z values.

2.2 HiKE-IMS-MS operational details

The same E/N was applied in both the ionisation source/reaction and drift regions and increased from 30 Td up to 115 Td in sequential steps of 5 Td. The ion gates at the end of the reaction and drift regions were left open so that ions were constantly transferred from the reaction region into the drift region of the drift tube, and from there into the ToF–MS for m/z identification. Maximum ion transfer was achieved by keeping both ion gates open. This was needed to get sufficient ion intensities into the ToF–MS identify the reagent and product ions with a high level of confidence. (A more detailed description of this operational procedure can be found in a paper by Allers et al. [9].) Each mass spectrum was acquired for 90 s, and each associated mass spectral peak in that spectrum was fitted to a Gaussian so that its peak position and its area could be accurately determined (especially important when overlapping spectral features occurred). For each E/N value, a mass spectrum was recorded three times and the determined peak areas were averaged.

2.3 Air supply

Purified dried sample and drift air flows were provided from a zero-air generator (JAG, JAGZAG600S). Prior

to entering the HiKE-IMS, the air had passed sequentially through a pressure swing absorber (Parker, K-MT 3 LAB), a moisture trap (< 1 ppm$_\mathrm{v}$ water) and a hydrocarbon filter. Unfortunately, owing to unavoidable diffusion through seals, our so-called *dry* purified air had a higher moisture content than that coming through the moisture trap. To avoid variations in the HiKE-IMS measurements and for what we will define as *dry* (low humidity) conditions, the humidity in the IMS was intentionally set to provide a water volume-mixing ratio of ~ 100 ppm$_\mathrm{v}$, corresponding to a residual relative humidity (rH) of $\sim 0.5\%$. For the higher humidity studies, the air was bubbled through a wash bottle filled with distilled water to achieve a rH $\sim 80\%$ for the sample air entering the ionisation source/reaction region.

The drift gas was independently supplied using the relatively dry air ($\sim 0.5\%$ rH), regardless of whether the sample air was introduced as "*dry*" or "*humid*" into the ionisation source/reaction region. Thus, in the following, the term *dry* refers to the investigations where, in the ionisation source/reaction region of the HiKE-IMS, the sample air was supplied at $\sim 0.5\%$ rH, and *humid* refers to the case for when the sample air entering the ionisation source/reaction region was at $\sim 80\%$ rH.

2.4 Chemicals

Acetone (CAS: 67–64-1), acetone-d$_6$ (CAS: 666–52-4), acetonitrile-d$_3$ (CAS: 2206–26-0), methanol (CAS: 67–56-1), methanol-d$_4$ (CAS: 811–98-3), ethanol (CAS: 64–17-5), ethanol-d$_1$ (CAS: 925–93-9), ethanol-d$_6$ (CAS: 1516–08-1), 2-propanol (CAS: 67–63-0), 2-propanol-d$_8$ (CAS: 22739–76-0), 1-butanol (CAS: 71–36-3) and 1-butanol-d$_{10}$ (CAS: 34193–38-9) were all purchased from Sigma-Aldrich. Acetonitrile (CAS: 75–05-8) was separately purchased from Supelco. All of these chemicals had stated purities of $> 99\%$, and were used without further purification. The isotopically labelled compounds had stated purities of $> 99.8\%$ atomic deuterium.

2.5 Sampling procedure

The compounds investigated were individually filled into low density-polyethylene pipettes (Baxter), which were sealed by welding the tap. These pipettes were placed into a temperature-controlled screw-cap tube, which was connected to the inlet capillary of the ionisation source/reaction region of the HiKE-IMS. The temperature was kept at a constant value, which, depending on the volatility of the compound, was somewhere between 35 and 45 °C in order to achieve comparable evaporation rates. Through this method, volatile volume mixing ratios in the range of approximately 5 ppm$_\mathrm{v}$ were achieved, which resulted in good product ion signal intensities, whilst retaining much of the reagent ion signals. However, for a number of the volatiles, the volatile volume mixing ratios were not sufficiently low

enough to stop the production of dimer or even trimer-containing product ions, as will be discussed further below.

3 Results and discussion

Crucial to improving our understanding of the primary ion-chemistry occurring in the HiKE-IMS is the identification and intensities of the reagent ions present in the reaction region under various operating conditions. Here this refers to differences in humidity levels of the sample air and the value of E/N. As mentioned earlier, E/N is a crucial HiKE-IMS operational parameter that determines (drift) reaction times and collisional energies, with the collisional energies being described by the Wannier equation. We will begin with a brief discussion of the reagent ions. More detailed information on their formation can be found in other recent HiKE-IMS papers [9, 10, 12].

3.1 Reagent ion distributions between 30 and 115 Td under dry and humid sample air conditions in the ionisation source/reaction region

The reagent ions present in the reaction region of the HiKE-IMS, and hence ions that can participate in the soft chemical ionisation of trace VOCs, include $H_3O^+(H_2O)_n$ (n = 0, 1, 2, and 3), $NO^+(H_2O)_m$ (m = 0, 1) and $O_2^{+\cdot}$ (as measured by the detector of the ToF–MS). Their distributions and relative intensities as a function of E/N and at the two humidities used in this study are presented in Figs. 1a, b, c, d and e.

We comment that in standard atmospheric pressure IMS systems operating in positive ion mode with an undoped buffer gas, protonated water clusters are the dominant reagent ions. These result from the high operational pressures and the associated longer reaction times (milliseconds rather than microseconds) that are a consequence of the low E/N values ($\sim$1–2 Td) applied. When using air as the buffer gas, $O_2^{+\cdot}$ ions are completely converted to $H_3O^+(H_2O)_q$ (q = 1, 2, 3, ...). NO^+ containing reagent ions are also converted to some extent to non-containing NO^+ ions. Via three body association processes $NO^+(H_2O)_3$ is formed, which undergoes thermoneutral intermolecular rearrangement ending up at protonated water clusters and neutral HNO_2.

The lower drift pressures in the HiKE-IMS result in the high E/N values. The amount of conversion of the $NO^+(H_2O)_m$ and $O_2^{+\cdot}$ ions depends not only on the value of E/N applied, but also the humidity of the sample air. Increasing E/N and decreasing humidity leads to reduced reaction times and less collisions with water, respectively, thereby limiting conversion. This is described in more detail in a couple of recent HiKE-IMS-MS publications that deal with an investigation of fundamental ion–molecule chemistry in a HiKE-IMS system [10, 13]. The explanation of the observations

Fig. 1 HiKE-IMS-MS reagent positive ion percentage distributions using **a**, **b** and **c** *d*ry and **d-e** *humid* sample air flows in the ionisation source/reaction region and **a-e** *dry* air in the drift region of the drift tube as a function of the reduced electric field. For clarity, the three types of reagent ions, namely $H_3O^+(H_2O)_n$, $NO^+(H_2O)_m$ and $O_2^{+\cdot}$ have been shown separately. To determine the percentage distributions, no allowance has been made for any m/z transmission dependencies
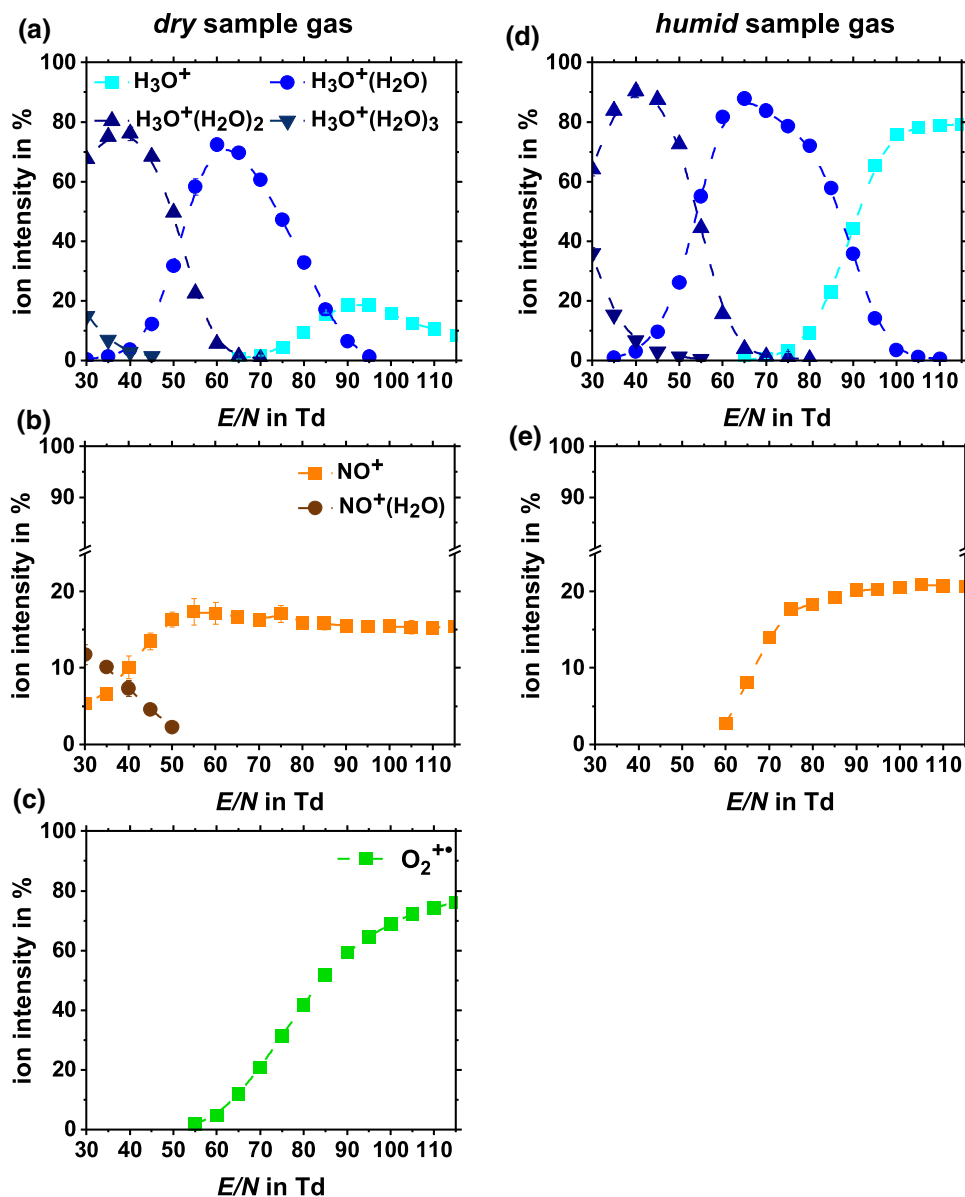
described in those HiKE-IMS-MS papers is based on work on the ion–molecule chemistry of the upper atmosphere, with key figures being Ferguson, Fehsenfeld, Arnold, Kebarle and Viggiano, amongst others [14–22].

In addition to reduced ion conversion, increasing E/N also has an effect on the distributions of the $H_3O^+(H_2O)_n$ and $NO^+(H_2O)_m$ reagent ions, because of the associated increase in collision-induced dissociation, which determines the corresponding water cluster sizes and hence distribution. Above about 90 Td, the water-containing reagent ions are predominantly H_3O^+ (Fig. 1a and d). Above about 50 Td, bare NO^+ ions (Fig. 1b and e) are observed. The *dry* sample air results in $O_2^{+\cdot}$ being the dominant reagent ion above about 80 Td, whereas in the *humid* sample air no $O_2^{+\cdot}$ is detected. Instead, protonated water monomers and clusters dominate, with NO^+ making a contribution of about 20% to the total reagent ion signal for E/N values

above about 70 Td. Hence, when using *humid* sample air, and only in terms of the reagent ions being present, the HiKE-IMS system becomes more like a traditional IMS system, but with the cluster sizes being heavily influenced by the value of the E/N used. Furthermore, and unlike traditional IMS, where reagent and product ions are essentially thermalized, the translational energies of the ions in the HiKE-IMS are strongly dependent on the E/N value. Therefore, with increasing humidity, for E/N greater than about 90 Td a change in the ion chemistry occurs, from being dominated by charge transfer to being dominated by ligand switching and proton transfer processes. This has significance in terms of use HiKE-IMS for the analytical analysis of humid air samples, such as real-time breath-to-breath sampling.

As mentioned above, $O_2^{+\cdot}$ is observed for the *dry* sample air conditions only, with a detectable signal being observed from about 55 Td onwards (Fig. 1 (c)).

At lower E/N values (< 55 Td) for the *dry* sample air (and at all E/N values investigated for the humid sample air), $O_2^{+\cdot}$ is converted to $H_3O^+(H_2O)_n$.

The conversion of $O_2^{+\cdot}$ is the major cause for the dramatic rise in the percentage of H_3O^+ with increasing E/N, observed for the *humid* sample air, reaching approximately 80% of the total reagent ion signal by about 100 Td. In comparison, when using *dry* sample air, H_3O^+ contributes only about 20% to the total reagent ion signal at approximately 90 Td. Another cause for the rise in the protonated water intensities in the humid air case comes from the higher water concentration leading to more protonated water and protonated water clusters being formed in the ionisation source. Collisions of the protonated water clusters with the neutral air molecules can lead to their declustering, the amount of which again depends on the value of E/N applied.

We mention here that in addition to $H_3O^+(H_2O)_n$, $NO^+(H_2O)_m$ and $O_2^{+\cdot}$ being formed in the ionisation region, two other reagent ions were observed in the mass spectra. These were NO_2^+ (m/z 46) and $O_4^{+\cdot}$ (m/z 64). However, they only have small ion intensities compared to the other reagent ions (individually they contribute $< 1\%$ to the total reagent ion signal at any E/N value investigated). Hence, at best they can only play a minor role in the ion chemistry occurring within the reaction region of the HiKE-IMS. Therefore, their ion distributions are not shown in Fig. 1.

3.2 Product ion distributions between 30 and 115 Td under dry and humid sample air conditions

The dependencies of the product ion intensities on E/N are illustrated in Figs. 2–7, under the two humidity conditions investigated. Table 1 summarises the measurements at three E/N values (30 Td, 80 Td and 115 Td), which cover the full range used. This table provides a quantitative indication of the importance of the various individual channels that were observed in this study. Furthermore, in order to illustrate and summarise the type of ion–molecule processes that can occur (primary and secondary processes), including proton transfer, hydride anion transfer, charge transfer and subsequent D/H exchange, Fig. 8 provides a reaction scheme for methanol-d_4. The identification of a product ion to a particular reagent ion is aided by comparing the *dry* to the *humid* sample air results, as illustrated below.

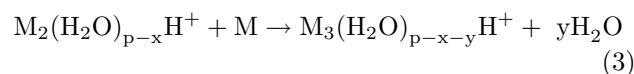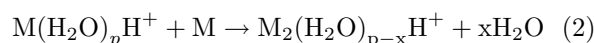### 3.2.1 *Product ions resulting from the reactions with $H_3O^{\cdot+}(H_2O)_n (n = 0, 1, 2,$ or $3)$*

The proton affinities (PAs) of the compounds (M) investigated in this study are all greater than that of water (PA = 691 kJ mol^{-1}) [23], and, with the exception of acetone (PA = 812 kJ mol^{-1} [23]), are all less than that of the water dimer (PA = 808 kJ mol^{-1}) [24]. Thus, proton transfer from H_3O^+ is exothermic for all compounds, and hence will proceed at the collisional rate coefficient. Proton transfer from $H_3O^+(H_2O)$ is

only facile for acetone. Instead, rapid ligand exchange reactions occur with the other volatiles, according to Eq. (1) [25], leading to water clustered protonated monomers of M:

$$M + H_3O^+(H_2O)_m \rightarrow M(H_2O)_pH^+ + ((m+1) - p)H_2O \tag{1}$$
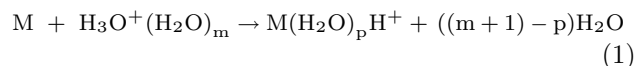
where m = 1, 2 and 3, and p = 0, 1 and 2. Once $M(H_2O)_pH^+$ ions are formed via ligand exchange reactions, collisions with neutral buffer gas the drift tube can lead to dissociation of the protonated monomer. These are particularly driven at high reduced electric field strengths.

Sequential reactions of $M(H_2O)_pH^+$ with M and H_2O may occur, leading to dimer (M_2) and trimer (M_3) containing product ions, as represented by Eqs. (2) and (3) [26], with their relative intensities being dependent of course on the concentration of M in the reaction region, the concentration of water in the drift tube, and the E/N value used throughout the drift tube (ionisation source/reaction and drift regions).

$$M(H_2O)_pH^+ + M \rightarrow M_2(H_2O)_{p-x}H^+ + xH_2O \tag{2}$$

$$M_2(H_2O)_{p-x}H^+ + M \rightarrow M_3(H_2O)_{p-x-y}H^+ + yH_2O \tag{3}$$

For simplicity, and because of the dependence of their relative intensities on the operational conditions, and the volatile and water concentrations, in Figs. 2, 3, 4, 5, 6 and 7 we have combined the product ions resulting from reactions (1)-(3) above, i.e., the sum of the monomer from ligand switching (1), and those of the dimer (2) and trimer (3) containing product ions.

In addition to the proton transfer and ligand switching reactions involving the protonated water containing ions, we comment that for the larger alcohols investigated, namely 2-propanol and 1-butanol, dissociative proton transfer leads to a loss of water resulting in the product ion $[M-H_2O]^+$ being formed. More specific comments on the reactions with the individual compounds are now discussed.

Acetonitrile/Acetonitrile-d_3

The primary reactions with protonated water species result in the formation of $(C_2H_3N)H^+$. This product ion can either be formed through rapid ligand switching with the protonated water clusters, and/or through direct proton transfer with H_3O^+. H_3O^+ is available as a reagent ion between 65 and 115 Td. Secondary association reactions with water and acetonitrile can then occur. The dimer and trimer containing product ions with one attached water are observed until about 35 Td under *dry* sample air conditions. With increasing E/N, collisional processes continuously reduce their intensities. The protonated dimer $(C_2H_3N)_2H^+$ is observed until about 80 Td. The protonated monomer $(C_2H_3N)H^+$ (m/z 42) is observed between 45 and 115 Td and becomes the dominant product ion above about 65 Td. From about 90 Td

Fig. 2 Product ion percentage distributions as a function of the reduced electric field for acetonitrile, C_2H_3N, and acetonitrile-d$_3$ using **a** and **c** purified *dry* and **b** and **d** *humid* sample air in the reaction region and **a-d** purified *dry* air in the drift region of the drift tube

Fig. 3 Product ion percentage distributions as a function of the reduced electric field for acetone, C_3H_6O, and acetone-d$_6$ using **a** and **c** purified *dry* and **b** and **d** *humid* sample air in the reaction region and **a-d** purified *dry* air in the drift region of the drift tube

Fig. 4 Product ion percentage distributions as a function of the reduced electric field for methanol, CH_3OH, and methanol-d_4 using **a** and **c** purified *dry* and **b** and **d** *humid* sample air in the reaction region and **a-d** purified *dry* air in the drift region of the drift tube
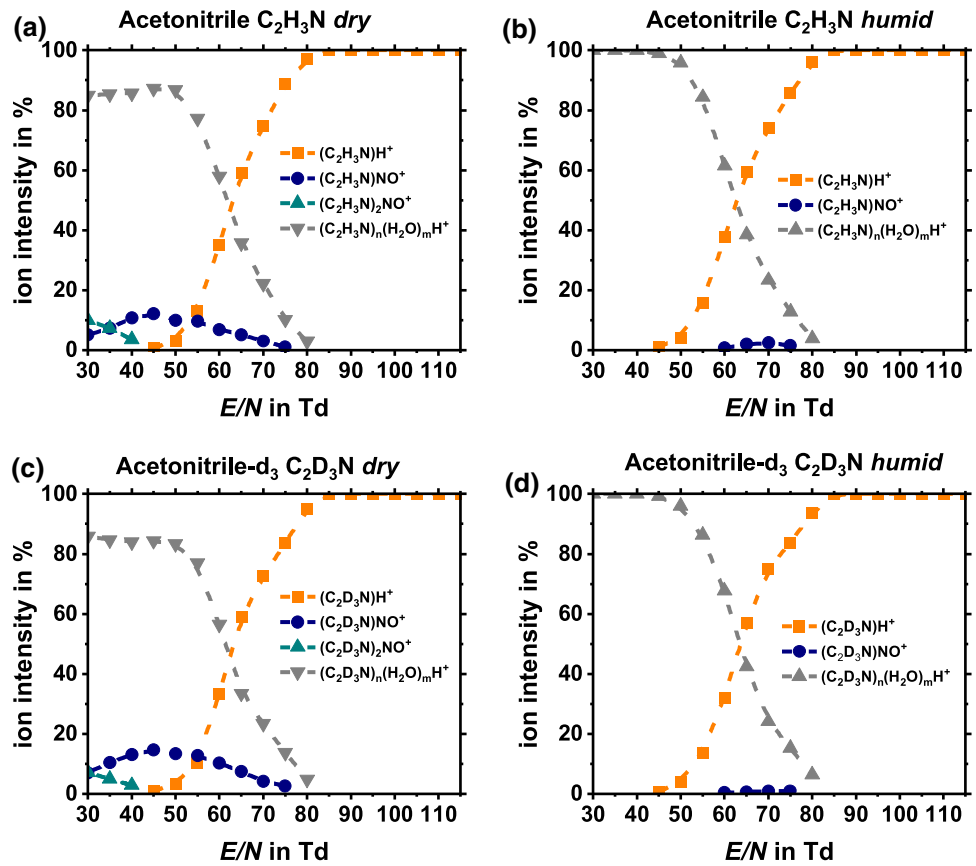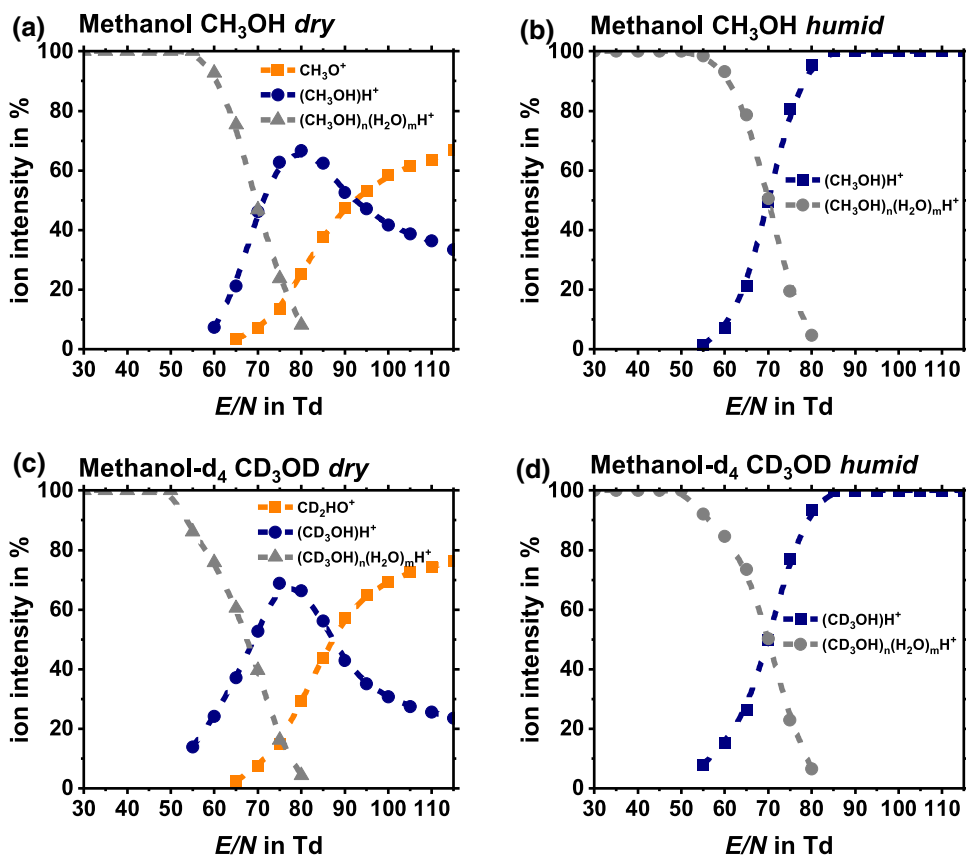

Fig. 5 Product ion percentage distributions as a function of the reduced electric field for ethanol, C_2H_5OH, and ethanol-d_6 using **a** and **c** purified *dry* and **b** and **d** *humid* sample air in the reaction region and **a-d** purified *dry* air in the drift region of the drift tube
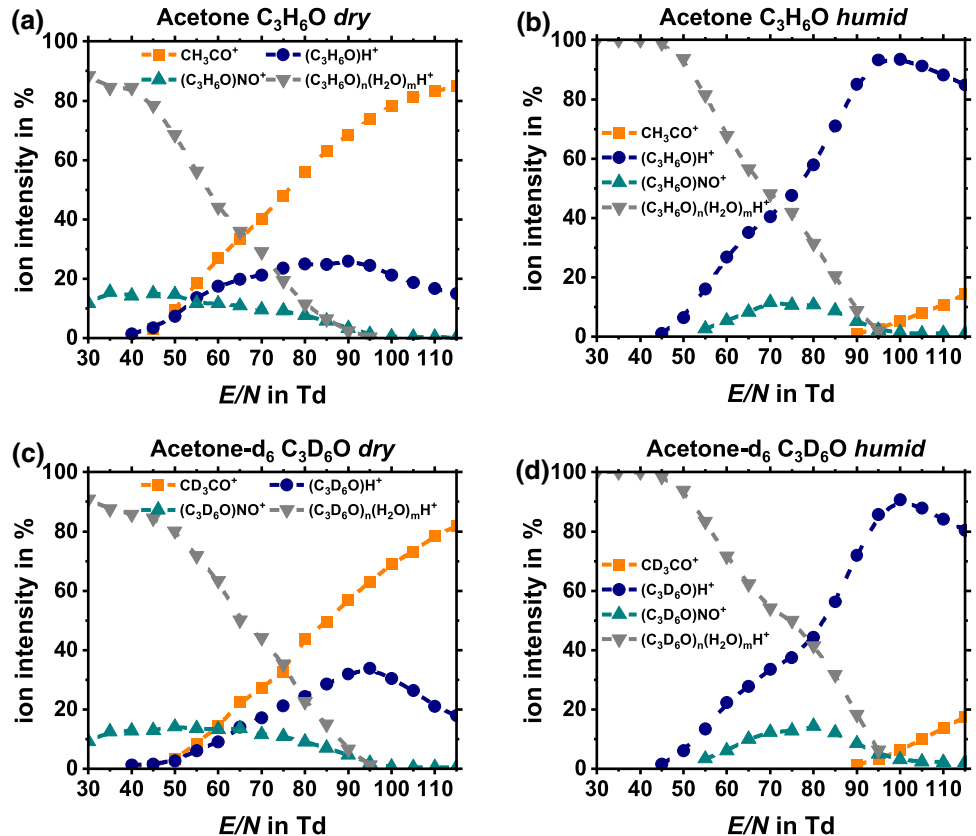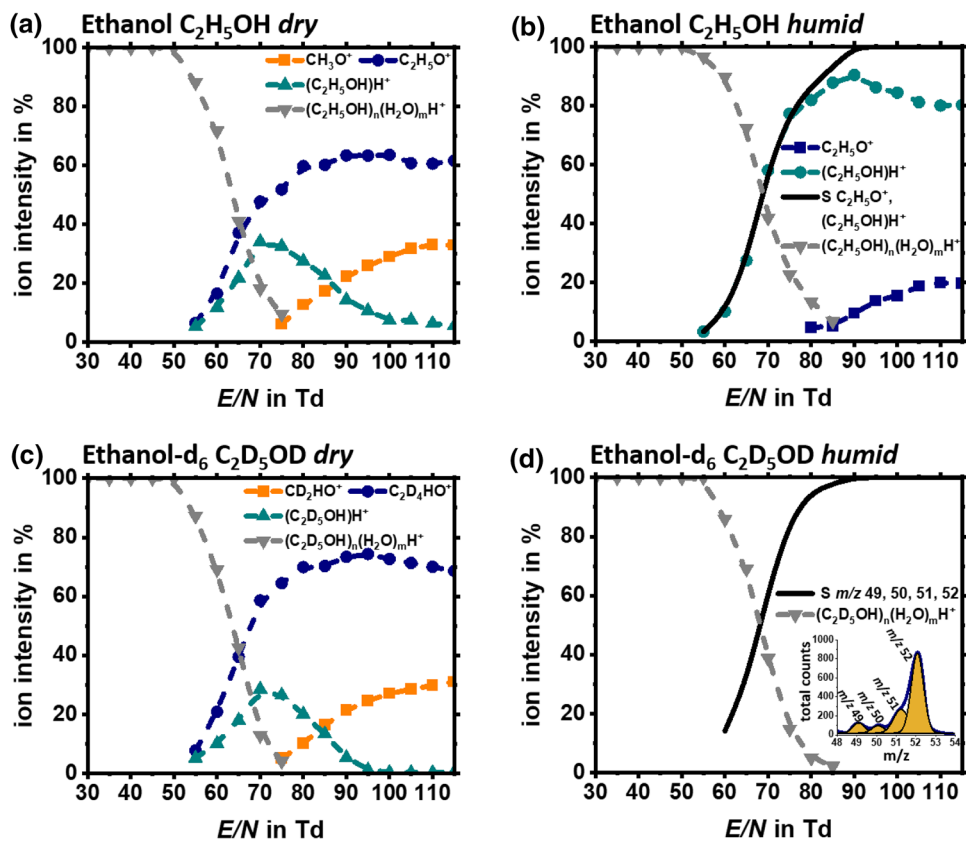
Fig. 6 Product ion percentage distributions as a function of the reduced electric field for 2-propanol, C_3H_7OH, and 2-propanol-d_8 using **a** and **c** purified *dry* and **b** and **d** *humid* sample air in the reaction region and **a-d** purified *dry* air in the drift region of the drift tube

Fig. 7 Product ion percentage distributions as a function of the reduced electric field for 1-butanol, C_4H_9OH, and 1-butanol-d_{10} using **a** and **c** purified *dry* and **b** and **d** *humid* sample air in the reaction region and **a-d** purified *dry* air in the drift region of the drift tube
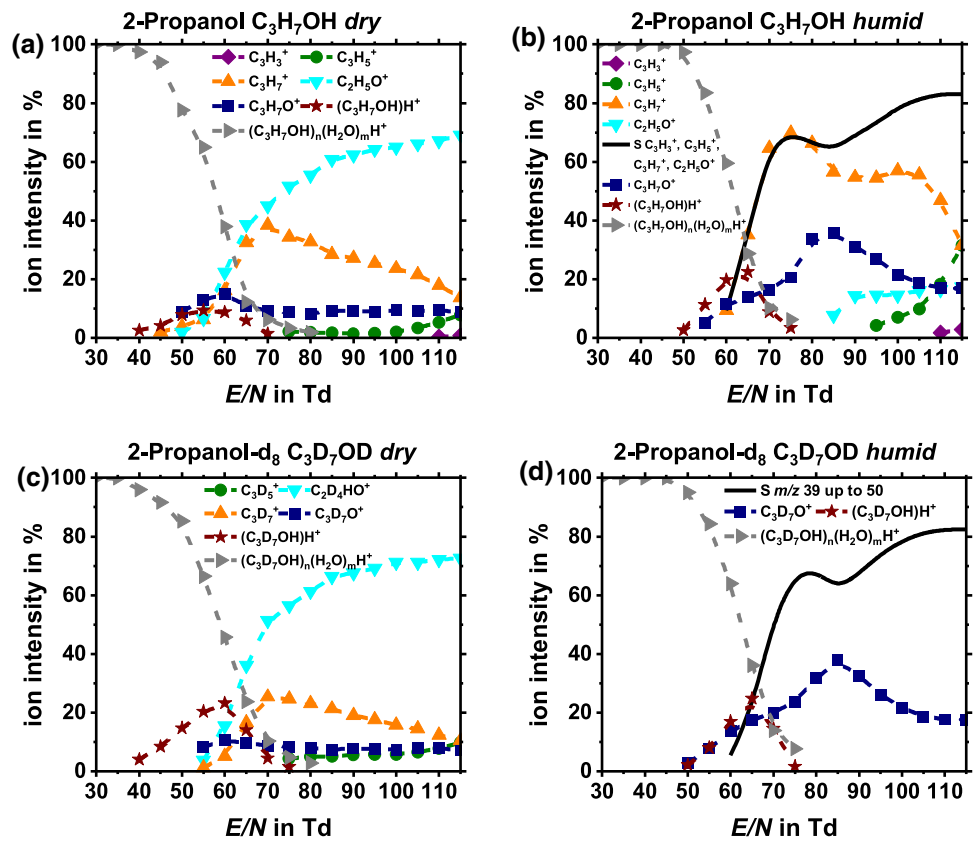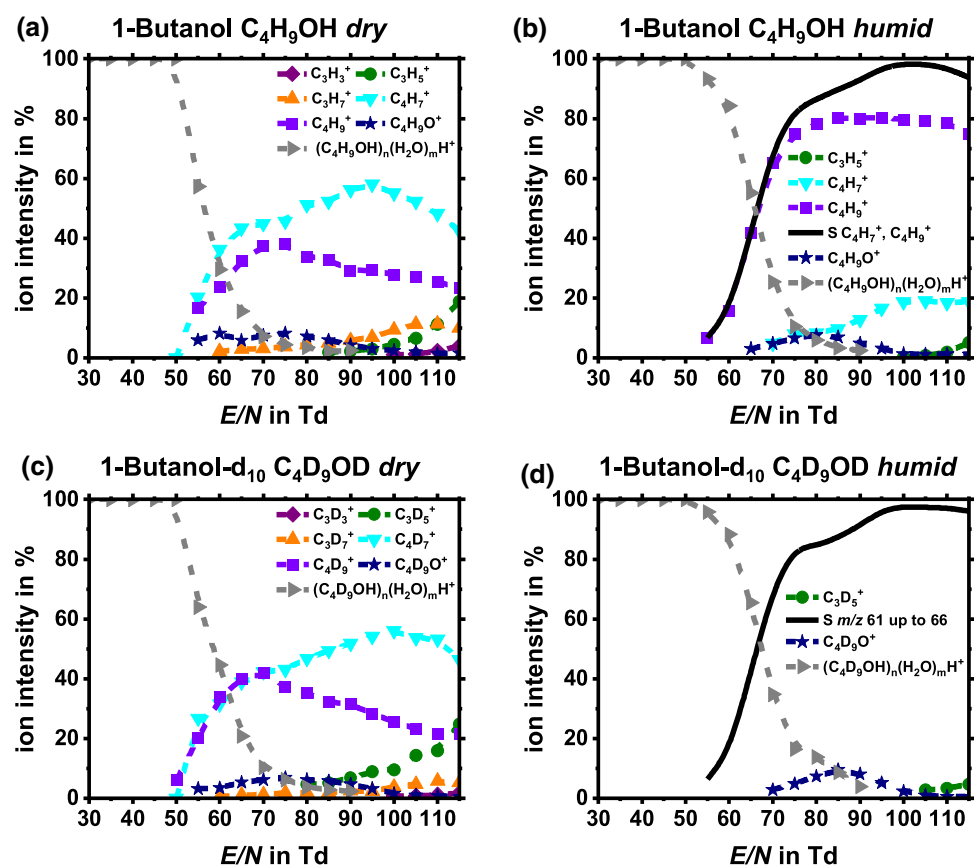
Table 1 Overview of the relative intensities (in percentages) of the identified product ions for the investigated compounds acetonitrile, acetonitrile-d$_3$, acetone, acetone-d$_6$, methanol, methanol-d$_4$, ethanol, ethanol-d$_6$, 2-propanol, 2-propanol-d$_8$, 1-butanol and 1-butanol-d$_{10}$. The data correspond to measurements taken at 30 Td, 80 Td and 115 Td for both dry and humid sample air conditions. The given percentages have been determined from three measurements. Errors in the branching percentages are conservatively estimated to be 10%

compound molecular formula lightest isotopomer	product ions (m/z)	E/N (Td) intensity % *dry* sample air			E/N (Td) intensity % *humid* sample air		
		30	80	115	30	80	115
Acetonitrile C$_2$H$_3$N 41.027	(C$_2$H$_3$N)$_3$(H$_2$O)H$^+$ (142)	11	–	–	1	–	–
	(C$_2$H$_3$N)$_2$NO$^+$ (112)	10	–	–	–	–	–
	(C$_2$H$_3$N)$_2$(H$_2$O)H$^+$ (101)	16	–	–	15	–	–
	(C$_2$H$_3$N)$_2$H$^+$ (83)	58	3	–	52	4	–
	(C$_2$H$_3$N)NO$^+$ (71)	5	–	–	–	–	–
	(C$_2$H$_3$N)(H$_2$O)H$^+$ (60)	–	–	–	32	–	–
	(C$_2$H$_3$N)H$^+$ (42)	–	97	100	–	96	100
Acetonitrile-d$_3$ C$_2$D$_3$N 44.045	(C$_2$D$_3$N)$_3$(H$_2$O)H$^+$ (151)	15	–	–	7	–	–
	(C$_2$D$_3$N)$_2$NO$^+$ (118)	7	–	–	–	–	–
	(C$_2$D$_3$N)$_2$(H$_2$O)H$^+$ (107)	14	–	–	26	–	–
	(C$_2$D$_3$N)$_2$H$^+$ (89)	57	5	–	37	6	–
	(C$_2$D$_3$N)NO$^+$ (74)	7	–	–	–	–	–
	(C$_2$D$_3$N)(H$_2$O)H$^+$ (63)	–	–	–	30	–	–
	(C$_2$D$_3$N)H$^+$ (45)	–	95	100	–	94	100
Acetone C$_3$H$_6$O 58.042	(C$_3$H$_6$O)$_2$H$^+$ (117)	88	11	–	98	31	–
	(C$_3$H$_6$O)NO$^+$ (88)	12	8	–	–	11	1
	(C$_3$H$_6$O)(H$_2$O)H$^+$ (77)	–	–	–	2	–	–
	(C$_3$H$_6$O)H$^+$ (59)	–	25	15	–	58	85
	CH$_3$CO$^+$ (43)	–	56	85	–	–	14
Acetone-d$_6$ C$_3$D$_6$O 64.079	(C$_3$D$_6$O)$_2$H$^+$ (129)	91	23	–	98	42	–
	(C$_3$D$_6$O)NO$^+$ (94)	9	9	–	–	14	2
	(C$_3$D$_6$O)(H$_2$O)H$^+$ (83)	–	–	–	2	–	–
	(C$_3$D$_6$O)H$^+$ (65)	–	24	18	–	44	81
	CD$_3$CO$^+$ (46)	–	44	82	–	–	17
Methanol CH$_3$OH 32.026	(CH$_3$OH)$_3$H$^+$ (97)	9	–	–	–	–	–
	(CH$_3$OH)$_2$(H$_2$O)H$^+$ (83)	30	–	–	–	–	–
	(CH$_3$OH)(H$_2$O)$_2$H$^+$ (69)	37	–	–	100	–	–
	(CH$_3$OH)$_2$H$^+$ (65)	20	8	–	–	–	–
	(CH$_3$OH)(H$_2$O)H$^+$ (51)	4	–	–	–	5	–
	(CH$_3$OH)H$^+$ (33)	–	67	33	–	95	100
	CH$_3$O$^+$ (31)	–	25	67	–	–	–

Table 1 (continued)

compound molecular formula lightest isotopomer	product ions (m/z)	E/N (Td) intensity % *dry* sample air			E/N (Td) intensity % *humid* sample air		
		30	80	115	30	80	115
Methanol-d$_4$ CD$_3$OD 36.051	(CD$_3$OH)$_3$H$^+$ (106)	9	–	–	–	–	–
	(CD$_3$OH)$_2$(H$_2$O)H$^+$ (89)	26	–	–	–	–	–
	(CD$_3$OH)(H$_2$O)$_2$H$^+$ (72)	30	–	–	100	–	–
	(CD$_3$OH)$_2$H$^+$ (71)	26	5	–	–	–	–
	(CD$_3$OH)(H$_2$O)H$^+$ (54)	9	–	–	–	7	–
	(CD$_3$OH)H$^+$ (36)	–	66	24	–	93	100
	CD$_2$HO$^+$ (33)	–	29	76	–	–	–
Ethanol C$_2$H$_5$OH 46.042	(C$_2$H$_5$OH)$_3$H$^+$ (139)	10	–	–	–	–	–
	(C$_2$H$_5$OH)$_2$H$^+$ (93)	33	–	–	11	–	–
	(C$_2$H$_5$OH)(H$_2$O)$_2$H$^+$ (83)	39	–	–	71	–	–
	(C$_2$H$_5$OH)(H$_2$O)H$^+$ (65)	18	–	–	18	13	–
	(C$_2$H$_5$OH)H$^+$ (47)	–	27	5	–	82	80
	C$_2$H$_5$O$^+$ (45)	–	60	61	–	5	20
	CH$_3$O$^+$ (31)	–	13	34	–	–	–
Ethanol-d$_6$ C$_2$D$_5$OD 52.079	(C$_2$D$_5$OH)$_3$H$^+$ (154)	20	–	–	–	–	–
	(C$_2$D$_5$OH)$_2$H$^+$ (103)	34	–	–	8	–	–
	(C$_2$D$_5$OH)(H$_2$O)$_2$H$^+$ (88)	32	–	–	75	–	–
	(C$_2$D$_5$OH)(H$_2$O)H$^+$ (70)	14	–	–	17	5	–
	(C$_2$D$_5$OH)H$^+$ (52)	–	20	1	–	84	100[1]
	C$_2$D$_4$HO$^+$ (49)	–	70	68	–	11	–
	CD$_2$HO$^+$ (33)	–	10	31	–	–	–
2-propanol C$_3$H$_7$OH 60.058	(C$_3$H$_7$OH)$_3$H$^+$ (181)	29	–	–	–	–	–
	(C$_3$H$_7$OH)$_2$H$^+$ (121)	44	2	–	24	–	–
	(C$_3$H$_7$OH)(H$_2$O)$_2$H$^+$ (97)	11	–	–	41	–	–
	(C$_3$H$_7$OH)(H$_2$O)H$^+$ (79)	16	–	–	35	–	–
	C$_3$H$_7$O$^+$ (59)	–	8	9	–	34	17
	C$_2$H$_5$O$^+$ (45)	–	55	69	–	–	17
	C$_3$H$_7^+$ (43)	–	33	14	–	66	32
	C$_3$H$_5^+$ (41)	–	2	7	–	–	31
	C$_3$H$_3^+$ (39)	–	–	1	–	–	3
2-propanol-d$_8$ C$_3$D$_7$OD 68.108	(C$_3$D$_7$OH)$_3$H$^+$ (202)	26	–	–	–	–	–
	(C$_3$D$_7$OH)$_2$H$^+$ (135)	47	3	–	33	–	–
	(C$_3$D$_7$OH)(H$_2$O)$_2$H$^+$(104)	7	–	–	35	–	–
	(C$_3$D$_7$OH)(H$_2$O)H$^+$(86)	20	–	–	32	–	–
	C$_3$D$_7$O$^+$ (66)	–	8	7	–	32	18
	C$_3$D$_7^+$ (50)	–	23	10	–	68[2]	82[2]
	C$_2$D$_4$HO$^+$ (49)	–	61	73	–	–	–
	C$_3$D$_5^+$ (46)	–	5	10	–	–	–

Table 1 (continued)

compound molecular formula lightest isotopomer	product ions (m/z)	E/N (Td) intensity % *dry* sample air			E/N (Td) intensity % *humid* sample air		
		30	80	115	30	80	115
1-butanol C_4H_9OH 74.073	$(C_4H_9OH)_3H^+$ (223)[3]	56	–	–	4	–	–
	$(C_4H_9OH)_2H^+$ (149)[3]	27	3	–	41	6	–
	$(C_4H_9OH)(H_2O)_2H^+$ (111)	8	–	–	41	–	–
	$(C_4H_9OH)(H_2O)H^+$ (93)	9	–	–	14	–	–
	$C_4H_9O^+$ (73)	–	7	2	–	8	1
	$C_4H_9^+$ (57)	–	34	23	–	78	75
	$C_4H_7^+$ (55)	–	51	42	–	8	19
	$C_3H_7^+$ (43)	–	5	10	–	–	–
	$C_3H_5^+$ (41)	–	–	19	–	–	5
	$C_3H_3^+$ (39)	–	–	4	–	–	–
1-butanol-d$_{10}$ C_4D_9OD 84.136	$(C_4D_9OH)_3H^+$ (250)[3]	62	–	–	2	–	–
	$(C_4D_9OH)_2H^+$ (167)[3]	27	4	–	46	14	–
	$(C_4D_9OH)(H_2O)_2H^+$ (120)	6	–	–	33	–	–
	$(C_4D_9OH)(H_2O)H^+$ (102)	5	–	–	19	–	–
	$C_4D_9O^+$ (82)	–	6	1	–	7	1
	$C_4D_9^+$ (66)	–	37	21	–	79[4]	94[4]
	$C_4D_7^+$ (62)	–	47	46	–	–	–
	$C_3D_7^+$ (50)	–	2	5	–	–	–
	$C_3D_5^+$ (46)	–	4	25	–	–	5
	$C_3D_3^+$ (42)	–	–	2	–	–	–

[1]No separation between m/z 49 and m/z 52
[2]No separation between m/z 39 and m/z 50
[3]Assignment above m/z 160 is prone to error owing to the poor mass resolution of the ToF–MS leading to very broad peaks. However, these are associated with secondary processes, which are not important in this study that is focused on investigating primary processes occurring in the HiKE-IMS
[4]No spectral separation between m/z 61 and m/z 66

onwards, $(C_2H_3N)H^+$ is formed only by proton transfer from H_3O^+, a reaction mechanism that is in agreement with that found in PTR-ToF–MS and SIFT-MS studies [27–29].

The same ion species mentioned above for unlabeled acetonitrile are also observed for acetonitrile-d$_3$, with approximately the same branching percentages under *dry* sample air operating conditions, namely $(C_2D_3N)_3(H_2O)H^+$ (m/z 151), $(C_2D_3N)_2(H_2O)H^+$ (m/z 107), $(C_2D_3N)_2H^+$ (m/z 89) and $(C_2D_3N)H^+$ (m/z 45) (Fig. 2 (c)). Moreover, $(C_2H_3N)(H_2O)H^+$ (m/z 60) $((C_2D_3N)(H_2O)H^+$ (m/z 63)) is observed from about 30 Td up to about 50 Td under the *humid* sample air conditions. These are formed from ligand switching reactions with protonated water clusters. Compared to the *dry* sample air, this shift in branching percentages simply reflects the changes in the relative volatile to water concentrations.

Acetone/Acetone-d$_6$

Protonated monomers $(C_3H_6O)H^+$ (m/z 59)/$(C_3D_6O)H^+$ (m/z 65) are either formed by direct proton transfer from H_3O^+ and $H_3O^+.H_2O$ (important above about 50 Td) or via ligand switching from reactions with $H_3O^+(H_2O)_n$ (n = 2 or 3), for reactions involving E/N less than about 50 Td. Association is facile at these lower E/N values, leading to the protonated bound dimer being the dominant product ion under both *dry* and *humid* sample air conditions. In addition, for the *humid* sample air, hydrated protonated monomers were also identified $((C_3H_6O)(H_2O)H^+$ (m/z 77)/$(C_3D_6O)(H_2O)H^+$ (m/z 83). Although observed with low intensities, their formation stands in good agreement with a study by Smith et al. [30], for which hydration was found to increase with increasing humidity.

Fig. 8 Reaction scheme for methanol-d$_4$ illustrating proton transfer (P.T.), hydride abstraction with NO$^+$ and charge transfer (C.T.) to O$_2^+$. Also shown is the deuterium hydrogen exchange reaction with H$_2$O at the hydroxy functional group of the alcohol and at the oxonium intermediate
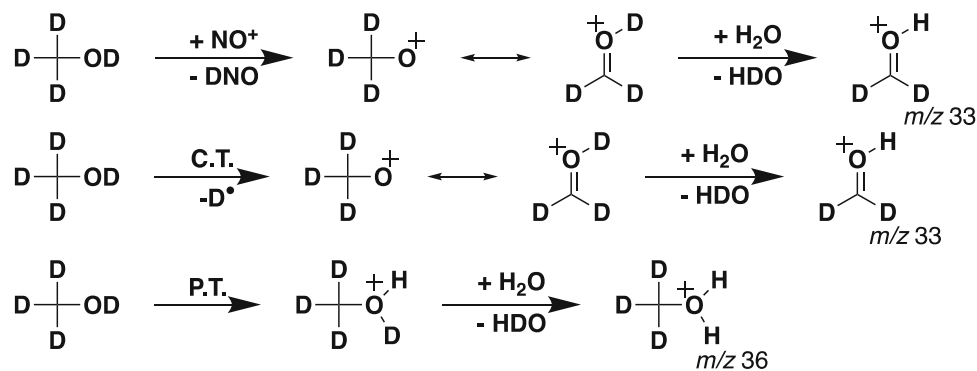
Above about 60 Td, reactions with H$_3$O$^+$ and H$_3$O$^+$(H$_2$O) are dominated by non-dissociative proton transfer. However, for the *humid* sample air, and from about 90 Td, another product ion is observed, CH$_3$CO$^+$/CD$_3$CO$^+$, which under *dry* sample air conditions is coming predominantly from dissociative charge transfer from reactions with O$_2^{+\cdot}$. Given that under *humid* sample air conditions no O$_2^{+\cdot}$ is available for reaction, this means that these product ions also result from reaction with NO$^+$ (see later).

The alcohols

Ligand switching (involving protonated water clusters) leads to the formation of (CH$_3$OH)H$^+$ (*m/z* 33) for methanol ((CD$_3$OH)H$^+$ (*m/z* 36) for methanol-d$_4$), (C$_2$H$_5$OH)H$^+$ (*m/z* 47) for ethanol ((C$_2$D$_5$OH)H$^+$ (*m/z* 52) for ethanol-d$_6$), (C$_3$H$_7$OH)H$^+$ (*m/z* 61) for 2-propanol ((C$_3$D$_7$OH)H$^+$ (*m/z* 68) for 2-propanol-d$_8$), and (C$_4$H$_9$OH)H$^+$ (*m/z* 75) for 1-butanol ((C$_4$D$_9$OH)H$^+$ (*m/z* 84) for 1-butanol-d$_{10}$), with or without water molecules being attached. However, note that these product ions are not necessarily directly observed, because of the formation of dimer and trimer containing product ions.

When H$_3$O$^+$ is present in sufficient concentrations, non-dissociative proton transfer directly occurs for methanol, ethanol and their associated deuterated compounds. Dissociative proton transfer results in the product ions C$_2$H$_5$O$^+$ (*m/z* 45) from ethanol (C$_2$D$_4$HO$^+$ (*m/z* 49) from ethanol-d$_6$), C$_3$H$_7$O$^+$ (*m/z* 59), C$_3$H$_7^+$ (*m/z* 43), C$_3$H$_5^+$ (*m/z* 41) and C$_3$H$_3^+$ (*m/z* 39) from 2-propanol (C$_3$D$_7$O$^+$ (*m/z* 66), C$_3$H$_7^+$ (*m/z* 50), and C$_3$D$_5^+$ (*m/z* 46) from 2-propanol-d$_8$), and C$_4$H$_9$O$^+$ (*m/z* 73) from 1-butanol (C$_4$D$_9$O$^+$ (*m/z* 82) from 1-butanol-d$_{10}$). However, it should be mentioned that contributions to these ions under *dry* sample air conditions also result from dissociative charge transfer processes involving O$_2^{+\cdot}$ (see later). That this occurs is obvious from a comparison of the product ion distributions between *dry* sample air (when significant levels of O$_2^{+\cdot}$ are available for reaction) and *humid* sample air (when no (or little) O$_2^{+\cdot}$ is available). Much of the results for the product ions obtained from this HiKE-IMS-MS study qualitatively agree at comparable E/N values with a PTR-(quadrupole) MS study reported by Brown et al. [31].

The protonated monomer of methanol (CH$_3$OH)H$^+$ (or (CD$_3$OD)H$^+$ for methanol-d$_4$, and detected as (CD$_3$OH)H$^+$) and ethanol (C$_2$H$_5$OH)H$^+$ (or (CD$_5$OD)H$^+$ for ethanol-d$_6$, and detected as (CD$_5$OH)H$^+$) are the dominant product ions above 70 Td under the *humid* sample air conditions. Below 70 Td hydrated proton bound monomers are formed. The proton bound dimer for ethanol (C$_2$H$_5$OH)$_2$H$^+$ is also observed below 70 Td.

Starting from the protonated monomer of 2-propanol (C$_3$H$_7$OH)H$^+$, a loss of H$_2$ results in the observed product ion C$_3$H$_7$O$^+$ (*m/z* 59), although with much higher branching percentages in this study than reported by Brown et al. This could be a result of the presence of NO$^+$ in our reaction region (see later). Elimination of H$_2$O from the protonated monomer leads to C$_3$H$_7^+$ (*m/z* 43) (or C$_3$D$_7^+$ for 2-propanol-d$_8$). Elimination of hydrogen from C$_3$H$_7^+$ is observed with increasing E/N, leading to the product ion C$_3$H$_5^+$ (or C$_3$D$_5^+$), and at the two highest E/N values investigated in this study, 110 and 115 Td, another hydrogen elimination is observed leading to the product ion C$_3$H$_3^+$. (Note C$_3$D$_3^+$ is not observed from the deuterated compound, which we attribute to the slightly lower vapor concentration of 2-propanol-d$_8$ used in that study leading to lower ion signals.)
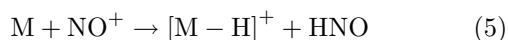
For 2-propanol (2-propanol-d$_8$), (C$_3$H$_7$OH)$_n$(H$_2$O)$_m$H$^+$ in Fig. 6 (b) ((C$_3$D$_7$HO)$_n$(H$_2$O)$_m$H$^+$ in Fig. 6 (d)) we include the protonated dimer (C$_3$H$_7$OH)$_2$H$^+$ (or (C$_3$D$_7$HO)$_2$H$^+$) and the hydrated protonated monomer (C$_3$H$_7$OH)(H$_2$O)$_{(1,2)}$H$^+$ (or (C$_3$D$_7$HO)(H$_2$O)$_{(1,2)}$H$^+$). A similar behavior in the product ion formation for a series of primary alcohols was also obtained within the SIFT-MS investigation of Spanel et al. [29]. An increase in humidity from 1.6 to 5.5% water vapor in their study was accompanied by an increased formation of the double hydrated proton bound monomer of 1-propanol (MH$^+$(H$_2$O)$_2$) from 18 to 58%.

A number of fragment product ions were detected between 50 and 115 Td for 1-butanol, which have also been reported in the PTR-MS study by Brown et al. [31]. These include C$_4$H$_9$O$^+$ (*m/z* 73), C$_4$H$_9^+$ (*m/z* 57), C$_4$H$_7^+$ (*m/z* 55), C$_3$H$_5^+$ (*m/z* 41), and C$_3$H$_3^+$ (*m/z* 39) (or for 1-butanol-d$_{10}$: C$_4$D$_9^+$ (*m/z* 66), C$_4$D$_7^+$ (*m/z* 62), C$_3$D$_5^+$ (*m/z* 46), and C$_3$D$_3^+$ (*m/z* 42)). However, under the dry sample air conditions,

contributions to these ions can also be coming from dissociative charge transfer (see the discussion of the $O_2^{+\cdot}$ results later). Elimination of H_2 from the protonated parent leads to the product ion $C_4H_9O^+$, whereas elimination of H_2O from the protonated parent results in $C_4H_9^+$ (or $C_4D_9^+$). H_2 (or D_2) elimination then results in $C_4H_7^+$ (or $C_4D_7^+$). The product ion $C_3H_5^+$ (or $C_3D_5^+$ for 1-butanol-d$_{10}$) is observed from about 100 Td. Note that the $(C_4H_9OH)_n(H_2O)_mH^+$ used in Fig. 7 includes the proton bound dimer and trimer containing ions $(C_4H_9OH)_2H^+$ and $(C_4H_9OH)_3H^+$) and increased ion intensities of the hydrated protonated monomers $(C_4H_9OH)(H_2O)_{(1,2)}H^+$, as also summarized in Table 1. The same discussion above applies to 1-butanol-d$_{10}$.

3.2.2 Product ions resulting from the reactions with NO$^+$

The recombination energy of NO$^+$ (9.26 eV) is less than the ionisation potentials of all of the compounds investigated, and hence this reagent ion cannot react with any of the volatiles via charge transfer. Instead, we observe adduct formation (Eq. (4) that requires a third body (B)) for reactions with acetonitrile and acetone, hydride ion abstraction leading to the formation of nitrosyl hydride [29] (Eq. (5)) for reactions with ethanol, 2-propanol, and 1-butanol, and hydroxide abstraction and nitrous acid formation for reactions with 2-propanol and 1-butanol (Eq. (6)).

$$M + NO^+ + B \rightarrow M \cdot NO^+ + B \qquad (4)$$

$$M + NO^+ \rightarrow [M - H]^+ + HNO \qquad (5)$$

$$M + NO^+ \rightarrow [M - OH]^+ + HNO_2 \qquad (6)$$

The last two Eqs. (5) and (6) are possible by the presence of an alcohol group. Except for methanol, where H$^-$ transfer is energetically not allowed, ethanol, 2-propanol and 1-butanol react via these pathways. According to Spanel et al. [32] for ethanol, H$^-$ is transferred in a tight ion/molecule complex ending up with CH_3CHOH^+, protonated acetaldehyde. For 2-propanol the hydride is taken from the carbon atom (and not the OH group). The energetic data is also provided by Spanel et al. [32]. The reaction pathways observed for specific volatiles are further discussed below.
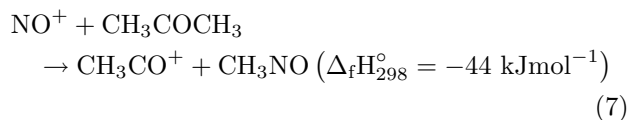
Acetonitrile/Acetonitrile-d3

Adduct formation of NO$^+$ with acetonitrile/ acetonitrile-d$_3$ leads to $(C_2H_3N)NO^+$ (m/z 71)/$(C_2D_3N)NO^+$ (m/z 74), with measurable intensities only between 30 and 75 Td. Adduct formation with this reagent ion has also been observed in a SIFT-MS study by Lehnert et al. [27]. However, in this study, between 30 and 40 Td, the dimer adduct ions, $(C_2H_3N)_2NO^+$ (m/z 112)/$(C_2D_3N)_2NO^+$ (m/z 118) have also been observed as a consequence of the high analyte concentration used. In the *humid* sample air measurements, the formation of $(C_2H_3N)NO^+$

(or $(C_2D_3N)NO^+$) starts at about 60 Td, i.e., at the E/N value for which NO$^+$ becomes available for reaction. These adducts are no longer viable under both *dry* and *humid* sample air conditions above about 75 Td, because collision-induced dissociation leads to their break-up.

Acetone/Acetone-d$_6$

Reactions of NO$^+$ with acetone and acetone-d$_6$ predominantly result in adducts via three body processes [30, 33, 34], leading to $(C_3H_6O)NO^+$ (m/z 88) and $(C_3D_6O)NO^+$ (m/z 94), respectively. An association reaction involving acetone and NO$^+$ was also reported in a SIFT-MS study by Rycroft et al. [35]. However, in that SIFT-MS study another product ion was observed, namely CH_3CO^+, with a product ion percentage of about 20%. Given that dissociative charge transfer would be highly endothermic, Rycroft et al. proposed that a short-range interaction resulted in the product ion through from the following pathway:

$$
\begin{aligned}
NO^+ &+ CH_3COCH_3 \\
&\rightarrow CH_3CO^+ + CH_3NO \left(\Delta_f H_{298}^\circ = -44 \text{ kJmol}^{-1}\right)
\end{aligned}
\qquad (7)
$$

However, given that this product ion was not reported in the other SIFT-MS studies, another explanation for the CH_3CO^+ is that NO$^+$ was internally excited in the study of Rycroft et al. The production of CH_3CO^+ under our *humid* sample air conditions is only possible from reactions involving NO$^+$ as the reagent ion. Whilst, we cannot rule out that NO$^+$ is not internally excited in our HiKE-IMS study, it is more probable that collisional processes are driving the dissociative charge transfer reaction pathway. Certainly, collisional induced dissociation of acetone.NO$^+$ leading to $C_3H_6O^+$ (+ NO) and CH_3CO^+ (+ CH$_3$/NO) has been reported in a SIFDT-MS study [36]. A difference in the formed product ions can of course result from the different operating pressures. The pressure difference between HiKE-IMS and SIFT-MS is approximately a factor of ten, which can result in differences in the product ion distributions when three body processes are important.

The Alcohols

No reaction of NO$^+$ with the simplest alcohol, methanol is observed, not even association, which was observed in a SIFT-MS study by Spanel et al. [32]. This can be explained by the higher product ion – neutral collisional energies in the HiKE-IMS, compared to the thermal collisional energies that take place in the flow tube of the SIFT-MS. Although H$^-$ transfer leading to CH_2OH^+ + HNO is endothermic at 300 K by only about 20 kJ mol^{-1} [34], the reaction is not found to be driven by the non-thermal collisional conditions in the HiKE-IMS.

The product ions $C_2H_5O^+$ (m/z 45) from ethanol $(C_2D_4HO^+$ (m/z 49) from ethanol-d$_6$), $C_3H_7O^+$ (m/z

59) from 2-propanol ($C_3D_7O^+$ (m/z 66) from 2-propanol-d$_8$) and $C_4H_9O^+$ (m/z 73) from 1-butanol ($C_4D_9O^+$ (m/z 82) for 1-butanol-d$_{10}$) are predominantly formed by hydride ion transfer to NO$^+$. (Contributions via dissociative proton transfer from H_3O^+ also occur and hence contribute to the intensities of these product ions (see above).) These observed product ions agree with a SIFT-MS study reported by Spanel et al. [32] for which [M-H]$^+$ was observed as a product ion resulting from the reaction of NO$^+$ with ethanol (100%), 2-propanol (100%) and 1-butanol (> 95%). In addition to the dominant product ion $C_4H_9O^+$, for 1-butanol the product ion $C_4H_9^+$ was observed resulting from OH$^-$ (hydroxide ion) abstraction, but its intensity was always less than 5% of the total product ion signal.

3.2.3 *Product ions resulting from reactions with $O_2^{+\cdot}$*

The recombination energy of $O_2^{+\cdot}$ (12.07 eV) is greater than the ionisation energies of acetone (9.703 eV), methanol (10.84 eV), ethanol (10.41 eV), 2-propanol (10.17 eV), and 1-butanol (9.99 eV). Hence, charge transfer to these compounds, represented by M in Eq. (8), is exothermic, and radical site-initiated fragmentation of the excited [M$^{+\cdot}$]* may occur leading to the formation of a fragment ion (F$^+$) and a free radical (R$^\cdot$) (Eq. (9)).

$$M + O_2^{+\cdot} \rightarrow \left[M^{+\cdot}\right] * + O_2 \tag{8}$$

$$\left[M^{+\cdot}\right]^* \rightarrow F^+ + R^\cdot \tag{9}$$
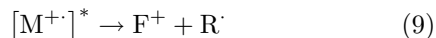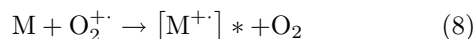
Recall that $O_2^{+\cdot}$ is only detected as a reagent ion when *dry* sample air is used. Under *humid* sample air conditions, once formed, $O_2^{+\cdot}$ is rapidly lost owing to its rapid conversion to $H_3O^+(H_2O)_n$. However, although it is not observed in the mass spectra, this does not rule out that some $O_2^{+\cdot}$ is available for reaction with volatiles under the high humid conditions, especially at the start of the reaction region. Nevertheless, we can assume that the majority of the product ions observed under *humid* sample air conditions are predominantly coming from reactions involving the reagent ions $H_3O^+(H_2O)_n$ and NO$^+$.

Acetonitrile/acetonitrile-d$_3$

The ionisation energy of acetonitrile (12.20 eV) is slightly greater than that of oxygen by about 0.13 eV. Although charge transfer is only slightly endothermic, it is found not to be driven by increasing the value of the reduced electric field. Thus, owing to the lack of reactions with $O_2^{+\cdot}$, changes in the product ion distributions between the *dry* and *humid* sample air conditions are expected to be limited for acetonitrile, and that is what is observed (see Fig. 2).

Acetone/acetone-d$_6$

Electron transfer from acetone to $O_2^{+\cdot}$ leads to the formation of the molecular radical cation, which rapidly dissociates leading to give the product ions CH_3CO^+ (m/z 43) (or CD_3CO^+ (m/z 46) for acetone-d$_6$) by radical site-initiated fragmentation:

$$C_3H_6O + O_2^{+\cdot} \rightarrow [C_3H_6O^{+\cdot}]^* + O_2 \rightarrow CH_3CO^+ + CH_3^\cdot + O_2 \tag{10}$$
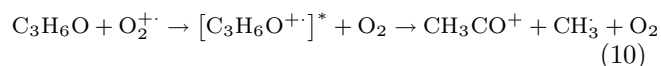
The non-dissociative charge transfer product ion is not observed in our study. This is distinctly different to the results obtained in the SIFT-MS investigations by Spanel et al. [33] and Smith et al. [37, 38]. $C_3H_6O^{+\cdot}$ and CH_3CO^+ were observed in both studies approximately in a ratio of 60:40, i.e., non-dissociative charge transfer was found to dominate under SIFT-MS conditions. The difference in the product ion distributions obtained in this HiKE-IMS-MS study must again result in the greater (non-thermal) translational energy the parent ion has, owing to the presence of the electric field in the drift tube. Collisional processes then lead to an effective internal ion temperature (vibrational and rotational) greater than thermal. This increase in internal energy leads to increased dissociation of the parent ion, which in turn leads to a different product ion distribution in HiKE-IMS-MS compared to that produced in the flow tube of a SIFT-MS.

The alcohols

The product ion CH_3O^+ (m/z 31) was observed from both methanol and ethanol (or CD_2HO^+ (m/z 33) for methanol-d$_4$ and ethanol-d$_6$), predominantly resulting from reactions with $O_2^{+\cdot}$, because the intensities of these ions dramatically decrease under the *humid* sample air conditions. CH_3O^+ could either result from dissociative charge transfer or from H$^-$ transfer resulting in neutral HO$_2$ [32]. Non-dissociative charge transfer leading to CH_3OH^+ and O_2 cannot be ruled out because its nominal m/z is the same as that for $O_2^{+\cdot}$, and hence cannot be detected.

Dissociative charge transfer also leads to the product ion $C_2H_5O^+$ (m/z 45) for both ethanol and 2-propanol. For 2-propanol this is a result of a loss of a methyl group:

$$C_3H_7OH + O_2^{+\cdot} \rightarrow [C_3H_7OH^{+\cdot}]^* + O_2 \rightarrow C_2H_5O^+ + CH_3^\cdot \tag{11}$$
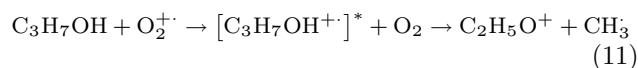
These observations agree with the PTR-MS results of Brown et al. [31] and the SIFT-MS results of Spanel et al. [32] and Wang et al. [39]. Under our *humid* sample air conditions, $C_2H_5O^+$ (or $C_2D_4HO^+$) is significantly reduced in intensity for both ethanol and 2-propanol (and their deuterated compounds), because no $O_2^{+\cdot}$ is available for reaction, but $C_2H_5O^+$ is still observed with a branching percentage of about 20% for $E/N > 90$ Td. This must be a result of a reaction with NO$^+$ for 2-propanol and dissociative proton transfer for ethanol under the *humid* sample air conditions.

The dominant product ion resulting from the reaction of $O_2^{+\cdot}$ with 1-butanol is observed to be $C_4H_7^+$ (m/z 55). $C_4H_7^+$ was not observed in a SIFT-MS study investigating the reaction of $O_2^{+\cdot}$ with 1-butanol [32], instead $C_4H_8^+$ (m/z 56) is the reported dominant species with a branching percentage of 80%. We assume that the lack of $C_4H_8^+$ in our study is yet again a result of the non-thermal collisional processes. Other product

ions we have observed from the reaction of $O_2^{+\cdot}$ with 1-butanol (1-butanol-d$_{10}$) in the HiKE-IMS are $C_3H_7^+$ ($C_3D_7^+$), $C_3H_5^+$ ($C_3D_5^+$) and $C_3H_3^+$ ($C_3D_3^+$).

D/H Exchange   Data presented in Table 1 and Figs. 4–7c and d show that significant D/H exchange does occur for the deuterium containing product ions. No such exchanges are observed for acetonitrile-d$_3$ and acetone-d$_6$, owing to their inert methyl functional group (–CD_3). This is in good agreement with the results of a PTR-ToF–MS study by Mochalski et al. [8].

An example of the D/H exchange reaction mechanism has been added in Fig. 8 for methanol-d$_4$. The figure also includes the primary reactions involving proton transfer with H_3O^+, hydride abstraction with NO^+, and dissociative charge transfer with $O_2^{+\cdot}$. D/H exchange for product ions coming from methanol-d$_4$ is obvious by the lack of any product ion containing four deuterium atoms. Instead, CD_3OH containing product ions are observed. Similarly, no CD_3O^+ ion resulting from the dissociative charge transfer reaction with $O_2^{+\cdot}$ is observed. This is because a D/H exchange leads to the product ion CD_2OH^+ being formed.

D/H exchange processes are also observed for ethanol-d$_6$, but the individual ions could not be completely resolved owing to the poor resolution of the mass spectrometer we had available for this investigation. For this reason, the ion signal intensities for ethanol and ethanol-d$_6$ have been qualitatively compared. To achieve this, the areas of $C_2H_5O^+$ and $(C_2H_5OH)H^+$ for ethanol were summed up and, in the case of ethanol-d$_6$, the areas for the ions with m/z 49, 50, 51, and 52 were estimated. To illustrate this, the mass spectrum for ethanol-d$_6$ at 80 Td is added into Fig. 5d. "S" in Fig. 5b and d indicates the sum of the areas, illustrated as a black line in each figure.

Similarly, only a qualitative comparison can be provided for 2-propanol and 2-propanol-d$_8$ in Figs. 6b and d, respectively. For 2-propanol the sum (S) of $C_2H_5O^+$, $C_3H_7^+$, $C_3H_5^+$ and $C_3H_3^+$ is formed and illustrated by the black line in the figure. For 2-propanol-d$_8$, the areas representing the various product ions between m/z 39 up to m/z 50 was estimated. The progressions of both black lines in Fig. 6b for 2-propanol and Fig. 6d for 2-propanol-d$_8$ are qualitatively the same. Although a full identification is not possible owing to the ToF–MS poor mass resolution in this present study, this observation nevertheless indicates that D/H exchange has occurred for the primary product ion $C_3D_7^+$, leading to ions with the general molecular formula $C_3D_nH_{7-n}^+$ ($n = 1$–6), as reported in the PTR-ToF–MS study of Mochalski et al. [8] for 2-propanol-d$_8$.

For 1-butanol-d$_{10}$, Figs. 7c and d and the results presented in Table 1 show that substantial D/H exchange also occurs at the hydroxy group.

The D/H exchange observed for the alcohols involves the carbonyl-bonded deuterium. The results therefore indicate that an exchange reaction is possible, when deuterium is bonded to an atom with higher electronegativity, which facilitates a nucleophilic attack of water. A more general reaction equation for the D/H exchange, with R being the corresponding alkyl rest of the investigated alcohols, is given in Eq. (12).

$$R - OD^+ + H_2O \rightarrow R - OH^+ + HDO \quad (12)$$
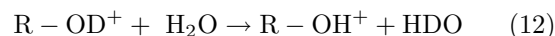
4 Concluding remarks

The HiKE-IMS-MS is a relatively new soft chemical ionisation spectrometric technique that is gradually being developed into an analytical chemistry tool. An analytical challenge results from the low pressures at which HiKE-IMS can operate ($\sim$ 10 to 40 mbar) leading to the presence of more than one type of reagent ion being present in the reaction region of the drift tube. This leads to more complex spectral data than obtained by either PTR-ToF–MS, SIFT-MS or IMS. However, this more complex spectral data could be exploited to enhance chemical specificity. To achieve this enhanced selectivity, the HiKE-IMS ion–molecule chemistry needs to be fully explored and understood. This highlights the need for studies, such as the one presented here, to further the development and applications of HiKE-IMS.

By investigating a series of volatiles and their completely deuterated analogues, and guided by the results from previous PTR-ToF–MS and SIFT-MS studies, the work presented in this paper has provided additional insights into the ion–molecule reaction processes occurring within the reaction region of the HiKE-IMS.

Whatever the cause of the differences in the product ion distributions between the various studies using different analytical instruments (e.g., HiKE-IMS-MS, PTR-ToF–MS, and SIFT-MS), this study highlights problems in obtaining comparable results, even when using similar soft chemical ionisation spectrometric technologies. Hence, for analytical purposes, each analytical instrument needs to be well characterized and calibrated for use in analytical chemistry applications.

Significant D/H exchange was observed to occur for the deuterium containing product ions coming from reactions involving the deuterated alcohols. These processes lead to more complex mass spectra, and hence reduce the intensity of the primary product ion. This unfortunately limits the use of deuterated compounds for use as isotopically labelled compounds in real-time breath volatile pharmacokinetic studies involving not only HiKE-IMS, but also PTR-ToF–MS and SIFT-MS, because of the high humidity associated with breath samples.

24146100), and in particular for the funding of Florentin Weiss's PhD programme and his exchange visit to Hannover in order to undertake the measurements presented in this paper. Furthermore, Hannover acknowledges the additional financial support of this project from the Deutsche Forschungsgemeinschaft (DFG, German Research Foundation) (318063177 and 390583968).

Author contribution

FW developed the methods, performed all the experiments, collected all of the data, analyzed the measurements, produced all of the figures and was involved in the writing of all drafts of the paper. GE, VR, and TM were involved in several scientific discussions and contributed to writing and reviewing the submitted draft. CAM suggested the project, took the lead in writing all of the drafts of the paper, and, with VR, supervised FW. CS and SZ were responsible for project administration in Hannover, and reviewed and agreed to the final draft of the paper.

Data Availability Statement This manuscript has no associated data or the data will not be deposited. [Authors' comment: This manuscript has no associated data or the data will not be deposited. The data that support the findings of this study are available within the article.]

Declarations

Conflict of interests The authors declare no conflict interests.

References

1. A. Amann, B.d.L. Costello, W. Miekisch, J. Schubert, B. Buszewski, J. Pleil, N. Ratcliffe, T. Risby, The human volatilome: volatile organic compounds (VOCs) in exhaled breath, skin emanations, urine, feces and saliva, J. Breath Res. 8:34001 (2014). https://doi.org/10.1088/1752-7155/8/3/034001.

2. Y.Y. Broza, P. Mochalski, V. Ruzsanyi, A. Amann, H. Haick, Hybrid volatolomics and disease detection. Angew. Chem. Int. Ed Engl. **54**, 11036–11048 (2015). https://doi.org/10.1002/anie.201500153

3. A. Bajtarevic, C. Ager, M. Pienz, M. Klieber, K. Schwarz, M. Ligor, T. Ligor, W. Filipiak, H. Denz, M. Fiegl, W. Hilbe, W. Weiss, P. Lukas, H. Jamnig, M. Hackl, A. Haidenberger, B. Buszewski, W. Miekisch, J. Schubert, A. Amann, Noninvasive detection of lung cancer by analysis of exhaled breath. BMC Cancer **9**, 348 (2009). https://doi.org/10.1186/1471-2407-9-348

4. K. Dixit, S. Fardindoost, A. Ravishankara, N. Tasnim, M. Hoorfar, Exhaled breath analysis for diabetes diagnosis and monitoring: relevance, challenges and possibilities. Biosensors (Basel) (2021). https://doi.org/10.3390/bios11120476

5. M. Stockmann, J.F. Lock, M. Malinowski, S.M. Niehues, D. Seehofer, P. Neuhaus, The LiMAx test: a new liver function test for predicting postoperative outcome in liver surgery. HPB (Oxford) **12**, 139–146 (2010). https://doi.org/10.1111/j.1477-2574.2009.00151.x

6. B. Braden, B. Lembcke, W. Kuker, W.F. Caspary, 13C-breath tests: current state of the art and future directions. Dig. Liver Dis. **39**, 795–805 (2007). https://doi.org/10.1016/j.dld.2007.06.012

7. V. Ruzsanyi, W. Lederer, C. Seger, B. Calenic, K.R. Liedl, A. Amann, Non-(13)CO2 targeted breath tests: a feasibility study. J. Breath Res. **8**, 46005 (2014). https://doi.org/10.1088/1752-7155/8/4/046005

8. P. Mochalski, S. Mirmigkou, K. Unterkofler, P. Sulzer, C.A. Mayhew, T.D. Märk, PTR-MS studies of the reactions of H3O+ with a number of deuterated volatile organic compounds and the subsequent sequential reactions of the primary product ions with water under normal and humid drift tube conditions: Implications for use of deuterated compounds for breath analysis. Int. J. Mass Spectrom. **436**, 65–70 (2019). https://doi.org/10.1016/j.ijms.2018.11.007

9. M. Allers, A.T. Kirk, N. von Roßbitzky, D. Erdogdu, R. Hillen, W. Wissdorf, T. Benter, S. Zimmermann, Analyzing positive reactant ions in high kinetic energy ion mobility spectrometry (HiKE-IMS) by HiKE-IMS-MS. J. Am. Soc. Mass Spectrom. **31**, 812–821 (2020). https://doi.org/10.1021/jasms.9b00087

10. M. Allers, A.T. Kirk, M. Eckermann, C. Schaefer, D. Erdogdu, W. Wissdorf, T. Benter, S. Zimmermann, Positive reactant ion formation in high kinetic energy ion mobility spectrometry (HiKE-IMS). J. Am. Soc. Mass Spectrom. **31**, 1291–1301 (2020). https://doi.org/10.1021/jasms.0c00114

11. A.T. Kirk, D. Grube, T. Kobelt, C. Wendt, S. Zimmermann, High-resolution high kinetic energy ion mobility spectrometer based on a low-discrimination tristate ion shutter. Anal. Chem. **90**, 5603–5611 (2018). https://doi.org/10.1021/acs.analchem.7b04586

12. C. Schaefer, M. Allers, A.T. Kirk, F. Schlottmann, S. Zimmermann, Influence of reduced field strength on product ion formation in high kinetic energy ion mobility spectrometry (HiKE-IMS). J. Am. Soc. Mass Spectrom. **32**, 1810–1820 (2021). https://doi.org/10.1021/jasms.1c00156

13. F. Weiss, C. Schaefer, V. Ruzsanyi, i. Märk, G. Eiceman, C.A. Mayhew, S. Zimmermann, High kinetic energy ion mobility spectrometry – mass spectrometry investigations of four inhalation anaesthetics: Isoflurane, enflurane, sevoflurane and desflurane, Int. J. Mass Spectrom. 116831 (2022). https://doi.org/10.1016/j.ijms.2022.116831.

14. A. Good, D.A. Durden, P. Kebarle, Mechanism and rate constants of ion-molecule reactions leading to formation of H + (H 2 O) n in moist oxygen and air. J. Chem. Phys. **52**, 222–229 (1970). https://doi.org/10.1063/1.1672668

15. Y.K. Lau, S. Ikuta, P. Kebarle, Thermodynamics and kinetics of the gas-phase reactions H3O+(H2O)n-1 + water = H3O+(H2O)n. J. Am. Chem. Soc. **104**, 1462–1469 (1982). https://doi.org/10.1021/ja00370a002

16. F.C. Fehsenfeld, M. Mosesman, E.E. Ferguson, Ion—Molecule Reactions in an O 2 +–H 2 O System. J. Chem. Phys. **55**, 2115–2120 (1971). https://doi.org/10.1063/1.1676382

17. F.C. Fehsenfeld, M. Mosesman, E.E. Ferguson, Ion—Molecule Reactions in NO + –H 2 O System. J. Chem. Phys. **55**, 2120–2125 (1971). https://doi.org/10.1063/1.1676383

18. E.E. Ferguson, Ion-Molecule Reactions in the Atmosphere, in *Kinetics of Ion-Molecule Reactions*. ed. by P. Ausloos (Springer, US, Boston, MA, 1979), pp.377–403

19. E.E. Ferguson, F. Arnold, Ion chemistry of the stratosphere. Acc. Chem. Res. **14**, 327–334 (1981). https://doi.org/10.1021/ar00071a001

20. E.E. Ferguson, F.C. Fehsenfeld, D.L. ALBRITTON, Ion chemistry of the earth's atmosphere, in: Gas Phase Ion Chemistry, Elsevier, 1979, pp. 45–82.

21. Handbook of atmospheric electrodynamics, CRC Press, Boca Raton, 1995.

22. N.S. Shuman, D.E. Hunton, A.A. Viggiano, Ambient and modified atmospheric ion chemistry: from top to bottom. Chem. Rev. **115**, 4542–4570 (2015). https://doi.org/10.1021/cr5003479

23. E.P.L. Hunter, S.G. Lias, Evaluated Gas Phase Basicities and Proton Affinities of Molecules: An Update. J. Phys. Chem. Ref. Data **27**, 413–656 (1998). https://doi.org/10.1063/1.556018

24. D.J. Goebbert, P.G. Wentold, Water dimer proton affinity from the kinetic method: dissociation energy of the water dimer. Eur. J. Mass Spectrom. (Chichester) **10**, 837–846 (2004). https://doi.org/10.1255/ejms.684

25. A.M. Ellis, C.A. Mayhew, *Proton Transfer Reaction Mass Spectrometry: Principles and Applications* (Wiley, Hoboken, 2013)

26. G.A. Eiceman, Z. Karpas, H.H. Hill, *Ion Mobility Spectrometry*, 3rd edn. (CRC Press, Boca Raton, Fla., 2014)

27. A.-S. Lehnert, T. Behrendt, A. Ruecker, G. Pohnert, S.E. Trumbore, Performance of SIFT-MS and PTR-MS in the measurement of volatile organic compounds at different humidities, Preprint. Discussion (2019) Atmospheric Measurement Techniques (Discussions) https://doi.org/10.5194/amt-2019-349

28. S.M. Abbott, J.B. Elder, P. Španěl, D. Smith, Quantification of acetonitrile in exhaled breath and urinary headspace using selected ion flow tube mass spectrometry. Int. J. Mass Spectrom. **228**, 655–665 (2003). https://doi.org/10.1016/S1387-3806(03)00212-4

29. P. Španěl, J. Žabka, I. Zymak, D. Smith, Selected ion flow tube study of the reactions of H3 O+ and NO+ with a series of primary alcohols in the presence of water vapour in support of selected ion flow tube mass spectrometry. Rapid Commun. Mass Spectrom. **31**, 437–446 (2017). https://doi.org/10.1002/rcm.7811

30. D. Smith, P. Španěl, K. Dryahina, H3O+, NO+ and O2+ reactions with saturated and unsaturated monoketones and diones; focus on hydration of product ions. Int. J. Mass Spectrom. **435**, 173–180 (2019). https://doi.org/10.1016/j.ijms.2018.10.027

31. P. Brown, P. Watts, T.D. Märk, C.A. Mayhew, Proton transfer reaction mass spectrometry investigations on the effects of reduced electric field and reagent ion internal energy on product ion branching ratios for a series of saturated alcohols. Int. J. Mass Spectrom. **294**, 103–111 (2010). https://doi.org/10.1016/j.ijms.2010.05.028

32. P. Spanel, D. Smith, SIFT studies of the reactions of H3O+, NO+ and O2+ with a series of alcohols. Int. J. Mass Spectrom. Ion Processes **167–168**, 375–388 (1997). https://doi.org/10.1016/S0168-1176(97)00085-2

33. P. Španěl, Y. Ji, D. Smith, SIFT studies of the reactions of H3O+, NO+ and O2+ with a series of aldehydes and ketones. Int. J. Mass Spectrom. Ion Processes **165–166**, 25–37 (1997). https://doi.org/10.1016/S0168-1176(97)00166-3

34. P. Španěl, D. Smith, A selected ion flow tube study of the reactions of NO + and O +2 ions with some organic molecules: The potential for trace gas analysis of air. J. Chem. Phys. **104**, 1893–1899 (1996). https://doi.org/10.1063/1.470945

35. L. Rycroft, T.A. Field, P. Scheier, C.A. Mayhew, Reactions of atomic and molecular ions with acetone, 1,1,1-trifluoroacetone, and hexafluoroacetone: An investigation of the effects of molecular structure on the dynamics and kinetics of ion–molecule reactions. Int. J. Mass Spectrom. **369**, 1–8 (2014). https://doi.org/10.1016/j.ijms.2014.04.014

36. A. Spesyvyi, D. Smith, P. Španěl, Ion chemistry at elevated ion-molecule interaction energies in a selected ion flow-drift tube: reactions of H3O+, NO+ and O2+ with saturated aliphatic ketones. Phys. Chem. Chem. Phys. **19**, 31714–31723 (2017). https://doi.org/10.1039/C7CP05795D

37. D. Smith, T. Wang, P. Spaněl, Analysis of ketones by selected ion flow tube mass spectrometry. Rapid Commun. Mass Spectrom. **17**, 2655–2660 (2003). https://doi.org/10.1002/rcm.1244

38. D. Smith, P. Spanel, Selected ion flow tube mass spectrometry (SIFT-MS) for on-line trace gas analysis. Mass Spectrom. Rev. **24**, 661–700 (2005). https://doi.org/10.1002/mas.20033

39. T. Wang, W. Carroll, W. Lenny, P. Boit, D. Smith, The analysis of 1-propanol and 2-propanol in humid air samples using selected ion flow tube mass spectrometry. Rapid Commun. Mass Spectrom. **20**, 125–130 (2006). https://doi.org/10.1002/rcm.2285